

Article

Characteristics and Source Apportionment of Size-Fractionated Particulate Matter at Ground and above the Urban Canopy (380 m) in Nanjing, China

Hao Wu¹, Pulong Chen², Tijian Wang^{3,*}, Min Xie³, Bingliang Zhuang³, Shu Li³ and Mengmeng Li³

¹ Key Laboratory of Transportation Meteorology of China Meteorological Administration, Nanjing Joint Institute for Atmospheric Sciences, Nanjing 210041, China; haowu@cma.gov.cn

² Jingling Era Jiangsu Environmental Technology Co., Ltd., Suzhou 215011, China; plchen@nju.edu.cn

³ School of Atmospheric Sciences, Nanjing University, Nanjing 210023, China; minxie@nju.edu.cn (M.X.); blzhuang@nju.edu.cn (B.Z.); lishu@nju.edu.cn (S.L.); mengmengli2015@nju.edu.cn (M.L.)

* Correspondence: tjwang@nju.edu.cn; Tel./Fax: +86-25-8968-3797

Abstract: In this study, the concentrations and chemical components of size-fractionated particulate matter (PM) in Nanjing at the ground (Gulou, 20 m) and above the urban canopy (Zifeng, 380 m) were sampled and analyzed from 16 November to 12 December in 2016. Higher concentrations of PM₁₀, PM_{10-2.1}, and PM_{2.1} ($108.3 \pm 23.4 \mu\text{g m}^{-3}$, $47.3 \pm 10.6 \mu\text{g m}^{-3}$, and $61.0 \pm 18.8 \mu\text{g m}^{-3}$) were measured at Gulou than those ($88.1 \pm 21.1 \mu\text{g m}^{-3}$, $31.4 \pm 6.7 \mu\text{g m}^{-3}$, and $56.7 \pm 18.6 \mu\text{g m}^{-3}$) at Zifeng. The most abundant chemical components for size-fractionated PM were SO₄²⁻, NO₃⁻, organic carbon (OC), NH₄⁺, elemental carbon (EC), and crustal elements such as Al, Ca, Fe, and Mg, varying significantly on different particulate sizes. The concentrations of OC and EC were 7.46–19.60 $\mu\text{g m}^{-3}$ and 3.44–5.96 $\mu\text{g m}^{-3}$ at Gulou and were 8.34–18.62 $\mu\text{g m}^{-3}$ and 2.86–4.11 $\mu\text{g m}^{-3}$ at Zifeng, showing an equal importance in both fine and coarse particles. Nitrate, sulfate, and ammonium were more concentrated in PM_{2.1}, contributing 11.30–13.76 $\mu\text{g m}^{-3}$, 8.91–9.40 $\mu\text{g m}^{-3}$, and 5.78–6.81 $\mu\text{g m}^{-3}$, which was more than in PM_{10-2.1}, which contributed 2.73–5.06 $\mu\text{g m}^{-3}$, 2.16–3.81 $\mu\text{g m}^{-3}$, and 0.85–0.87 $\mu\text{g m}^{-3}$. In contrast, the crustal elements were larger in coarse particles and at the ground level, accounting for 18.6% and 15.3% of the total PM at Gulou and Zifeng. Source apportionment using the chemical mass balance (CMB) model EPA showed that the dominant three sources were secondary nitrate (18.2–24.9%), secondary sulfate (14.5–20.4%), and secondary organic aerosols (15.5–19.6%) for PM₁₀, PM_{2.1}, and PM_{1.1} at both Gulou and Zifeng during the entire sampling period. However, for PM_{10-2.1}, the largest three contributors were secondary organic aerosols (18.3%), the coal-fired power plant (15.6%), and fugitive dust (14.4%), indicating dusts including construction dust, fugitive dust, and soil dust would contribute more at the ground. The results also showed that the concentrations of PM₁₀, PM_{2.1}, and PM_{1.1} were lower than the work carried out in the winter of 2010 at the same sampling site by 41.4%, 26.3%, and 24.8%, confirming the improvement of the air quality and the efficient control of PM pollutants.

Keywords: size-fractionated PM; chemical characteristics; source apportionment; ground level (20 m); urban canopy (380 m)



Citation: Wu, H.; Chen, P.; Wang, T.; Xie, M.; Zhuang, B.; Li, S.; Li, M. Characteristics and Source Apportionment of Size-Fractionated Particulate Matter at Ground and above the Urban Canopy (380 m) in Nanjing, China. *Atmosphere* **2022**, *13*, 883. <https://doi.org/10.3390/atmos13060883>

Academic Editors: Duanyang Liu, Kai Qin and Honglei Wang

Received: 8 May 2022

Accepted: 27 May 2022

Published: 29 May 2022

Publisher's Note: MDPI stays neutral with regard to jurisdictional claims in published maps and institutional affiliations.



Copyright: © 2022 by the authors. Licensee MDPI, Basel, Switzerland. This article is an open access article distributed under the terms and conditions of the Creative Commons Attribution (CC BY) license (<https://creativecommons.org/licenses/by/4.0/>).

1. Introduction

Nowadays, atmospheric particulate matter (PM) are receiving a lot of attention in atmospheric and environmental studies due to their complex and important impact on various problems, including human health [1,2], radiation balance and climate change [3–5], visibility degradation [6,7], and air pollution [8–10]. In recent decades, with increased economic and industrial development, PM have become the primary air pollutant in urban areas, and PM pollution, especially PM_{2.5} pollution (atmospheric particulate matter with an aerodynamic diameter less than 2.5 μm), has been found to be a severely impairing

issue in China. So, considerable attention from governments and scientific communities has been drawn [11–15] and lots of studies have been focused on the mass concentrations and chemical properties of particles [16,17]. The chemical compositions of atmospheric PM consist of numerous numbers of species (metals, ions, and carbonaceous matter) and come from complex sources, including anthropogenic and natural sources [18]. Meanwhile, the formation processes involve complicated multiphase formation pathways that are not well understood yet [19,20]. So, it is significant to understand the formation and contribution to PM mass in urban areas.

Many previous efforts have been conducted to evaluate the size distributions and chemical compositions at ground level (0~20 m), which is significantly influenced by local emission sources such as fugitive dust, construction dust, and vehicle exhaust. In comparison, an observation of size-fractionated particulate matter (PM) on a height of 300–400 m would be meaningful to understand the influences from a large scale of the sources, transportation, formation, and removal mechanisms to particulate matter [21–23]. Nanjing is a megacity located in the most developed region of the Yangtze River Delta in China with a huge population and a large urban center. It is a perfect target to carry out the ground level and high-height level observations. Characteristics and source contributions of atmospheric particles were discussed by previous studies in Nanjing [24,25], but the chemical compositions and sources of PM in different sizes at ground level and high-height level have not yet been conducted. As the nocturnal planetary boundary height during the winter is often about 300 m, we chose Zifeng Tower (380 m) in Nanjing to be the observation site of atmospheric particulate matter in the lower boundary layer [26].

Compared to developed countries, the emission sources of atmospheric particles in developing countries are much more complex. An explicit knowledge of the source contributions and probable source locations is the first step for understanding and planning management strategies of particulate matter [27]. The receptor model is used for quantitative analysis of PM source contributions, as there is no limitation on pollution discharge, weather conditions, or terrain factors. Based on chemical analysis, the receptor models that could be chosen are either the chemical mass balance (CMB) method or a multivariate factor analysis model such as the positive matrix factorization (PMF) method. Both methods have been widely applied to evaluate the particles' source contributions [28–31]. Source profiles are necessary in the former method but useless in the latter method. However, there is no limitation in the number of samples in the former method, but a minimum number of samples should be prescribed in the latter method. The source profiles in Nanjing were obtained in a previous work [18], and due to the limitation of sample numbers, the CMB model was used in this study. Additionally, backward trajectory clustering analysis could be used to trace the source locations of emissions [32]. Moreover, backward trajectory clustering analysis combined with the results of receptor models have been proved to be a beneficial tool for identifying the major source locations [33–35].

In this study, a synchronous and parallel observation was carried out at the ground level and the 380 m platform on Zifeng Tower in Nanjing from November to December in 2016. The mass concentrations of size-fractionated PM were obtained, and the chemical compositions including elements, water-soluble ions, and carbonaceous matter (elemental carbon (EC) and organic carbon (OC)) were analyzed. The size distribution of chemical components and variations between the ground level and the 380 m platform were investigated. The CMB model was applied to apportion the emission source contributions of PM in different sizes. The characteristics of source contributions at ground level and above the urban canopy (380 m) were evaluated. Combined with backward trajectory clustering analysis, the potential transport pathways were traced at the two heights. Finally, based on the results above, we explored reasonable control measures that may be helpful for policymakers.

2. Materials and Methods

2.1. Study Area and Sample Collection

Nanjing (118°22" and 119°14" E, 31°14" and 32°37" N) is the capital of Jiangsu province, the second largest city in the Yangtze River Delta. With rapid development in recent decades, vehicle exhaust, coal-fired power generation, and industrial activities have become the main anthropogenic sources of PM in Nanjing. The Gulou District is the urban center of Nanjing with huge population and heavy traffic. So, we chose the Gulou campus of Nanjing University and Zifeng Tower in this district to be the sampling sites. One of the sampling sites, Zifeng Tower, is a 450-meter skyscraper completed in 2010 in Nanjing, China. It is the tallest building in Jiangsu province, and the 10th tallest building in the world (as of August 2016). The observation instruments were located on the top platform at 380 m. Another set of observation instruments was located on the roof of a 20 m high building in Gulou campus, Nanjing University. The two observation points are close with a distance of less than 700 m. The locations of sampling sites are shown in Figure 1. The two sampling sites are represented as Gulou and Zifeng in the following text.

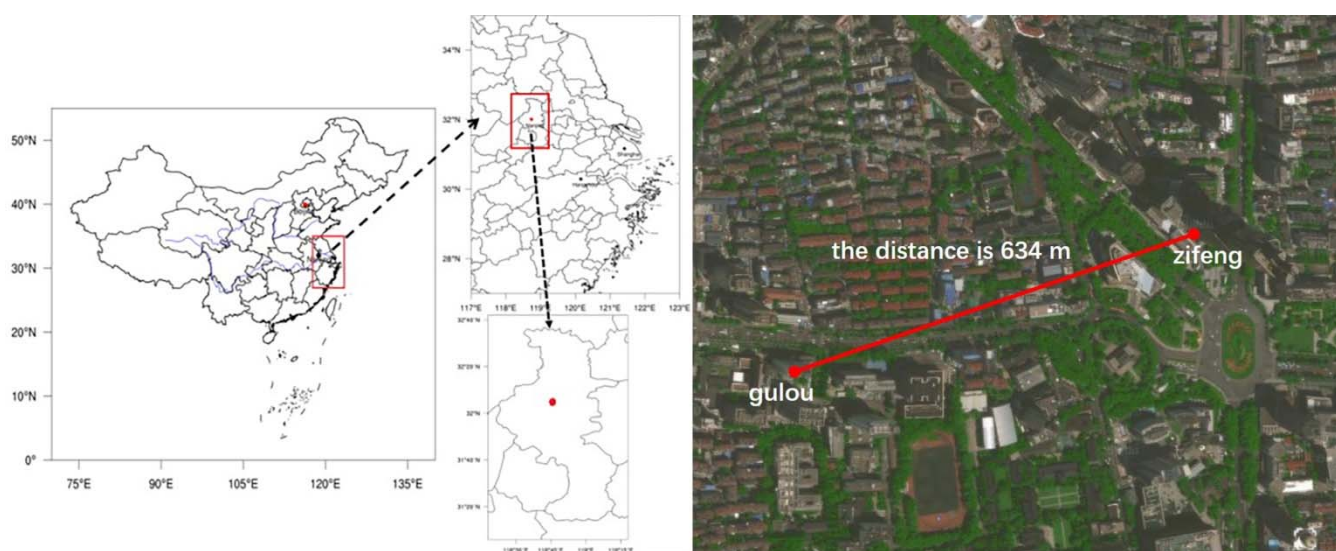


Figure 1. The locations of sampling sites.

The sampling campaign was carried out from 16 November to 12 December in 2016 at 20 m and 380 m height, except 28 November due to power failure at Gulou. During the experiment, size-fractionated ambient particulate matter (PM) were collected with an eight-stage Sierra-Andersen cascade impactor (Andersen Instruments, Inc., Atlanta, GA, USA), which can classify nine intervals in the following order: <0.43 μm , 0.43–0.65 μm , 0.65–1.1 μm , 1.1–2.1 μm , 2.1–3.3 μm , 3.3–4.7 μm , 4.7–5.8 μm , 5.8–9.0 μm , and 9.0–10 μm (aerodynamic diameter) [25,36]. Two parallel samplers with flow rate of 28.3 L min^{-1} were placed at each height in order to obtain chemical compositions of particles with Teflon-membrane filters and quartz fiber filters (Diameter 81 mm). Forty-seven hours of sampling was performed every two days from 9 am to 8 am and on the third day to obtain adequate materials at high level.

2.2. Chemical Analysis

Elements (e.g., Al, As, Ba, Ca, Cd, Co, Cr, Cu, Fe, K, Mg, Mn, Ni, P, Pb, Sn, Sr, Ti, V, and Zn), ions (e.g., F^- , CH_3COO^- , HCOO^- , Cl^- , NO_3^- , SO_4^{2-} , $\text{C}_2\text{O}_4^{2-}$, Na^+ , NH_4^+ , K^+ , $(\text{CH}_3)_2\text{NH}_2^+$, Ca^{2+} , Mg^{2+}), and carbonaceous materials (organic carbon (OC) and elemental carbon (EC)) were analyzed for each sample.

2.2.1. Analysis of Elements

Elements obtained from Teflon filters were analyzed by an inductively coupled plasma mass spectrometer (ICP-MS, Agilent Technologies, Inc., Model 7500a, Santa Clara, CA, USA). Calibration with reference material (Environmental Calibration Standard, Part 5183-4688, Agilent Technologies) demonstrated good linearity and sensitivity for the instrument. The relative standard deviation for each measurement (repeated twice) was within 3%. The method detection limits (MDLs) were determined by adding 3 standard deviations of the blank readings to the average blank values [26].

2.2.2. Analysis of Water-Soluble Ions

Water-soluble ions obtained from half of the quartz fiber filters were analyzed by an ion chromatography (IC, DIONEX Corporation, Model ICS-90, Sunnyvale, CA, USA). The IC was periodically checked with standard reference materials. The relative standard deviation for each measurement (repeated twice) was within 3%. The method detection limit (MDL) was provided by the ion chromatography manufacturer. Determination of inorganic cations and ammonium in environmental waters was performed by ion chromatography with a high-capacity cation-exchange column. The MDLs of cations were 22, 20, 5, 48, 6, and 48 ng/mL for Na^+ , NH_4^+ , K^+ , Mg_2^+ , Ca_2^+ , and $(\text{CH}_3)_2\text{NH}_2^+$, respectively. The MDLs of anions were 2, 4, 11, 9, 66, 7, and 15 ng/mL for F^- , Cl^- , NO_3^- , SO_4^{2-} , CH_3COO^- , HCOO^- , and $\text{C}_2\text{O}_4^{2-}$, respectively.

2.2.3. Analysis of Carbonaceous Materials

Carbonaceous materials (OC and EC) obtained from another half of the quartz fiber filters were analyzed by a thermal/optical carbon analyzer (DRI, Model 2001, Desert Research Institute, Reno, NV, USA) with the thermal/optical reflectance (TOR) method [37,38]. A circle piece of 0.53 cm^2 was cut off from the filters and was sent into the thermal optical carbon analyzer. A blank sample was analyzed for blank subtraction. Quality control and quality assurance procedures were routinely applied for all the elemental, ion, and carbonaceous analyses.

2.3. CMB Model

The chemical mass balance (CMB) receptor model was used in this study to apportion the source contributions to the size-fractionated PM at different heights. The EPA CMB 8.2 version (US EPA, 2004) with the effective variance weighted least-squares fitting method was applied. CMB is a widely used method for source apportionment of particulate matter. It consists of a solution to a set of linear equations that expresses each receptor chemical concentration as a linear sum of products of source profile abundances and source contributions. Source samples were collected and analyzed, and then profiles were determined for local representative emissions [18,26]. The chemical abundances are normalized to values between 0% and 100%.

$$C_{it} = \sum_{i=1}^N F_{in} S_{nt} + E_{it} \quad (1)$$

In Equation (1), C_{it} represents the ambient concentration of the i -th chemical species measured at time t . It is equal to the sum of the contributions from N sources, in theory. F_{in} is the fractional abundance (source profile) of the i -th species in the n -th source type. S_{nt} is the mass contribution of n -th source at time t . E_{it} represents the difference between the measured and estimated ambient concentration [25].

2.4. Cluster Analysis of Back Trajectories

The three-dimensional (latitude, longitude, and altitude) cluster analysis of back trajectories shows us the dominant transport pathways of air mass, which could reflect the potential influence of sources from a large scale during the sampling campaign. Trajectories were generated with version 4.9 of the NOAA Air Resources Laboratory's Hybrid Single-

Particle Lagrangian Integrated Trajectory (HYSPPLIT) model [39]. Archived meteorological data from the National Centers for Environmental Prediction (NCEP)/National Center for Atmospheric Research (NCAR) reanalysis project data set with 6 h intervals and a spatial resolution of $2.5 \times 2.5^\circ$ in longitude and latitude were used as input data to calculate 36 h trajectories starting at 20 m and 380 m, separately. During the observation periods, back trajectories were computed every three hours for each sampling day (00 h, 03 h, 06 h, 09 h, 12 h, 15 h, 18 h, and 21 h in UTC). Then, all the trajectories were clustered with HYSPPLIT clustering algorithm. The clustering of back trajectories is based on the total spatial variance (TSV) method [40], which minimizes the inter-cluster differences among trajectories.

Hourly weather data such as temperature (T), relative humidity (RH), wind speed (WS), and wind direction (WD) were obtained from an automatic weather station on the roof of a 20 m high building in Gulou campus, Nanjing University.

3. Results and Discussion

3.1. Size-Fractionated PM Mass Characteristics

During the sampling period, the average PM_{10} concentration was $108.3 \pm 23.4 \mu\text{g m}^{-3}$ and $88.1 \pm 21.1 \mu\text{g m}^{-3}$ at Gulou and Zifeng, respectively. The mean mass concentration of the PM_{10} concentration at ground level was 22.9% higher than that at high height (380 m), and the PM_{10} concentration at Gulou was higher at every sampling day than at Zifeng. The average $PM_{2.1}$ concentration was $56.7 \pm 18.6 \mu\text{g m}^{-3}$ with the range from $34.6 \mu\text{g m}^{-3}$ to $89.7 \mu\text{g m}^{-3}$ at Zifeng. The average $PM_{2.1}$ concentration was $61.0 \pm 18.8 \mu\text{g m}^{-3}$, ranging from $32.4 \mu\text{g m}^{-3}$ to $87.5 \mu\text{g m}^{-3}$ at Gulou, which was 7.6% higher than that measured at Zifeng. At specific sampling days, the mass concentrations of $PM_{2.1}$ were higher at high height (380 m). In contrast, the averaged mass concentration of $PM_{1.1}$ at Zifeng was $44.8 \pm 15.8 \mu\text{g m}^{-3}$, which was 9.5% higher than $40.9 \pm 13.0 \mu\text{g m}^{-3}$ at Gulou.

The more active secondary formation processes of aerosols at the higher level or the long-distance transportation from other regions may have caused these results, which will be explored and discussed in the following text. The coarse particles showed the same feature as PM_{10} at different heights. The summary statistics of measured PM_{10} , $PM_{10-2.1}$, $PM_{2.1}$, and $PM_{1.1}$ are presented in Table 1. The mass concentrations of PM_{10} , $PM_{2.1}$, and $PM_{1.1}$ in this study were 41.4%, 26.3%, and 24.8% lower than those in previous study at Gulou, Nanjing during winter 2010 [24]. Meanwhile, compared with the similar research in a megacity of North China from December 2013 to January 2014 [41], the mass concentrations of PM_{10} and $PM_{2.1}$ in Tianjin were 107.5% and 73.6% higher than those in this study. Overall, the air quality in Nanjing is better for these years, and a decrease trend of size-fractionated PM mass concentrations with increasing height was shown, except for $PM_{1.1}$.

Table 1. Statistics of measured PM_{10} , $PM_{10-2.1}$, $PM_{2.1}$, and $PM_{1.1}$ at Gulou and Zifeng ($\mu\text{g m}^{-3}$).

Site	Type	Mean	SD ^a	Max	Min
Gulou	PM_{10}	108.3	23.4	145.6	62.7
	$PM_{10-2.1}$	47.3	10.6	66.1	36.1
	$PM_{2.1}$	61.0	18.8	87.5	32.5
	$PM_{1.1}$	40.9	13.0	72.7	25.3
Zifeng	PM_{10}	88.1	21.1	124.1	56.5
	$PM_{10-2.1}$	31.4	6.7	41.9	21.8
	$PM_{2.1}$	56.7	18.6	89.7	34.6
	$PM_{1.1}$	44.8	15.8	79.4	27.1

^a Standard deviation.

Figure 2 shows the time series of observed size-fractionated PM mass concentrations at Gulou and Zifeng, which indicates that the time-scale variation trend was consistent at two heights. The correlation coefficient of PM_{10} , $PM_{10-2.1}$, and $PM_{2.1}$ between Gulou and Zifeng was 0.79, 0.86, and 0.73, respectively. Further, in order to study the variations of particulate

concentrations and chemical compositions, the coefficient of divergence (CD) [42,43] could be used as follows:

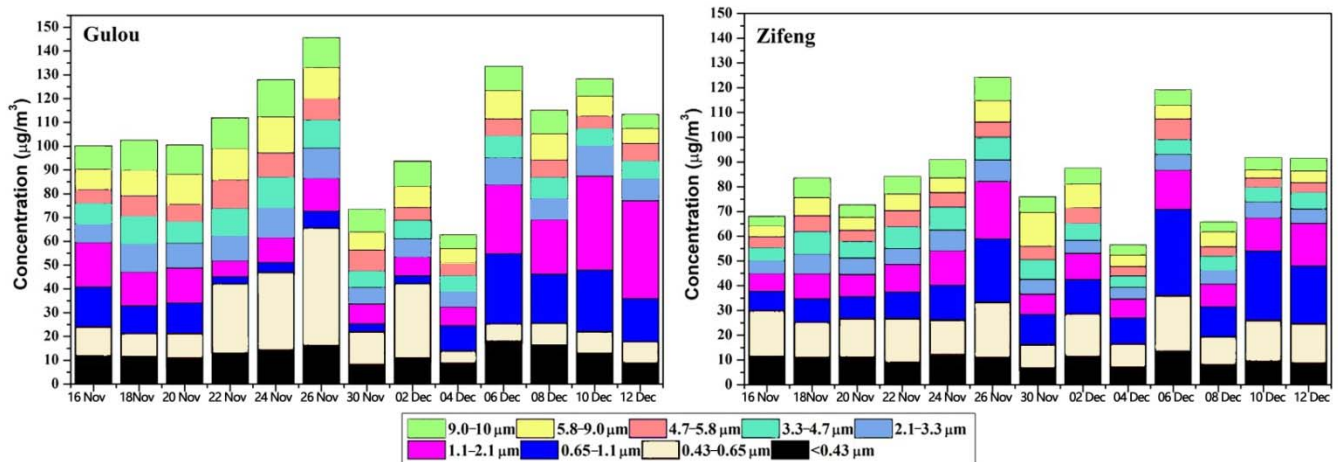


Figure 2. Time series of size-fractionated mass concentrations at Gulou (20 m) and Zifeng (380 m).

$$CD_{gz} = \sqrt{\frac{\sum_{n=1}^N (C_{ng} - C_{nz})^2}{C_{ng} + C_{nz}}} \quad (2)$$

where g and z represent the two sampling sites, and N is the total number of sampling days. C_{ng} or C_{nz} means mass concentrations at different sites in the n th day. The value of CD shows the similarity of the mass concentrations of particulate matter at the two sites. The lower value represents the stronger similarity. When the value of CD is zero, it means the mass concentrations at the two sites are the same [44]. In actual analysis, a CD value above 0.3 indicates a difference between each height, whereas a CD value less than 0.3 could be a sign of similarity between two heights [45]. To the mass concentrations, the values of CD for different particle sizes are shown in Table 2. All the CD values for PM_{10} , $PM_{10-2.1}$, $PM_{2.1}$, and $PM_{1.1}$ between Gulou and Zifeng are less than 0.3, which indicates that the mass concentrations of particles are similar at each height. The CD value of the $PM_{10-2.1}$ mass concentration is relatively higher than those of $PM_{2.1}$ and $PM_{1.1}$, which suggests that the coarse particulate matter presents a larger variation between 20 m and 380 m. This might imply that local and primary sources contributed more to coarse particles at the ground than high height.

Table 2. Coefficient of divergence (CD) of mass concentrations and main chemical compositions for size-fractionated PM between Gulou (20 m) and Zifeng (380 m).

Species	PM_{10}	$PM_{10-2.1}$	$PM_{2.1}$	$PM_{1.1}$
PM mass	0.139	0.220	0.097	0.096
Al	0.251	0.326	0.151	0.190
Ca	0.235	0.304	0.161	0.185
Fe	0.286	0.355	0.161	0.213
K	0.188	0.242	0.170	0.233
Mg	0.243	0.314	0.180	0.229
Cl	0.201	0.221	0.192	0.175
Na	0.172	0.185	0.290	0.324
NO_3^-	0.196	0.321	0.173	0.169
SO_4^{2-}	0.121	0.282	0.087	0.124
NH_4^+	0.195	0.405	0.130	0.117
OC	0.089	0.125	0.096	0.093
EC	0.245	0.424	0.212	0.210
CH_3COO^-	0.490	0.487	0.529	0.598
$HCOO^-$	0.206	0.230	0.126	0.165
$C_2O_4^{2-}$	0.278	0.117	0.425	0.464
$(CH_3)_2NH_2^+$	0.449	0.607	0.466	0.489

The sampling was conducted during November to December 2016, the most polluted time of the year. In this study, there is no 2.5 μm cut point, so 2.1 μm is defined as the threshold of fine particles, and the clear day standard for $\text{PM}_{2.5}$, which is less than $75 \mu\text{g m}^{-3}$ (Technical Regulation on Ambient Air Quality Index (HJ633-2012)), would be used for $\text{PM}_{2.1}$ here. During the whole sampling period, there were four samples exceeding $75 \mu\text{g m}^{-3}$ at the ground (26–27 November, 6–7 December, 10–11 December, and 12–13 December), and at Zifeng (380 m) there were two samples exceeding $75 \mu\text{g m}^{-3}$ (26–27 November and 6–7 December). According to previous work, the beginning, process, and dispersion of particulate pollution could be influenced or driven by meteorological conditions [46–48]. The weather data observed at Gulou (20 m) were discussed with the concentration level. The hourly series of meteorological conditions including temperature (T), relative humidity (RH), wind speed (WS), and wind direction (WD) were shown in Figure 3. Under the weather condition of low wind speed, the PM concentrations would increase. The concentrations of $\text{PM}_{2.1}$ at Gulou were higher than $75 \mu\text{g m}^{-3}$ in 26–27 November, 6–7 December, 10–11 December, and 12–13 December when the daily maximum wind speeds were 2.9 m/s, 2.8 m/s, 3.8 m/s, and 3.9 m/s, respectively. However, the lowest concentration of $\text{PM}_{2.1}$ was $32.5 \mu\text{g m}^{-3}$ in 4–5 December, with a much higher daily maximum wind speed (7 m/s). Additionally, the sampling day with low RH showed cleaner than the sampling day with high RH. The concentrations of $\text{PM}_{2.1}$ at Gulou in 26–27 November and 12–13 December with higher daily average RH (69.6% and 79.1%) were much larger than that in 4–5 December with lower daily average RH (60.0%).

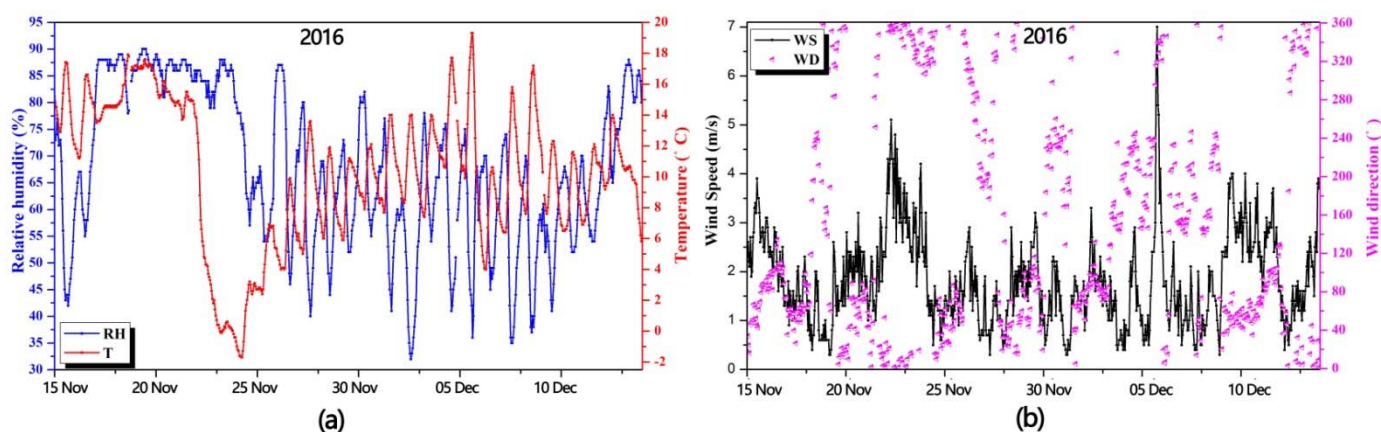


Figure 3. Time series of hourly (a) temperature and relative humidity and (b) wind speed and wind direction.

The average mass concentrations of size-fractionated PM manifested different features at different heights. The mass size distributions of PM with standard deviation at Gulou and Zifeng are shown in Figure 4. The distribution patterns of PM mass concentrations from 9.0–10 μm to 1.1–2.1 μm at two sites were similar, which showed an increasing trend with finer particulate size and the minimum concentration at 4.7–5.8 μm . However, the distribution patterns of particles smaller than the size bin of 1.1–2.1 μm were different. A bimodal distribution pattern could be found at Gulou with higher concentrations in the size bin of 1.1–2.1 μm and 0.43–0.65 μm . Otherwise, a unimodal distribution pattern could be found at Zifeng with a highest concentration in size bin of 0.43–0.65 μm . Particles in different sizes showed generally larger concentrations at Gulou than those at Zifeng, except in size bins of 0.65–1.1 μm and 0.43–0.65 μm , which caused the concentrations of $\text{PM}_{1.1}$ to be larger at 380 m than at the ground. The average ratios of $\text{PM}_{2.1}/\text{PM}_{10}$ at Gulou and Zifeng were 0.56 and 0.64, indicating that more fine particulate matter were contained in PM_{10} at high height. The average ratios of $\text{PM}_{1.1}/\text{PM}_{2.1}$ at Gulou and Zifeng were 0.67 and 0.79, indicating in wintertime that the fine particulate matter at the top of the boundary

layer were finer than those at the ground level. The ratios of $PM_{2.1}/PM_{10}$ and $PM_{1.1}/PM_{2.1}$ for each sampling day at Gulou and Zifeng are shown in Figure 4.

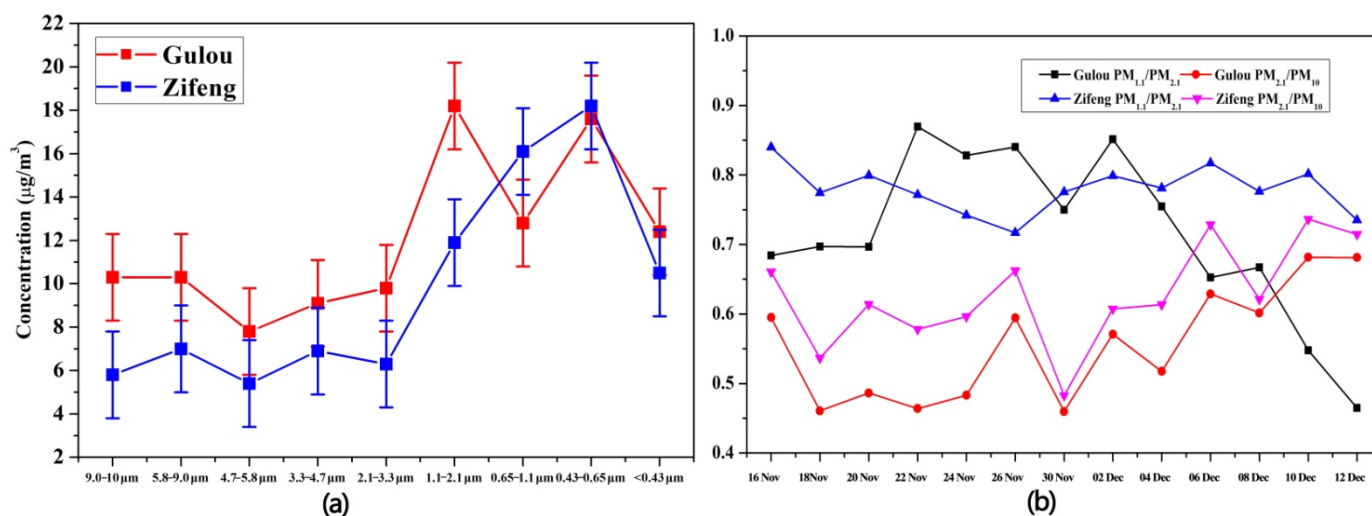


Figure 4. (a) The average mass size distributions of PM with standard deviation at Gulou (20 m) and Zifeng (30 m). (b) The ratios of $PM_{2.1}/PM_{10}$ and $PM_{1.1}/PM_{2.1}$ at Gulou and Zifeng.

3.2. Characteristics of Chemical Compositions

The size-fractionated PM are mainly composed of crustal elements, water-soluble ions, and carbonaceous matter. The average mass concentrations of the chemical components at each sampling height in PM_{10} , $PM_{10-2.1}$, $PM_{2.1}$, and $PM_{1.1}$ are shown in Table 3. The characteristics of chemical compositions are discussed in three sections containing elements, water-soluble ions, and carbonaceous matter.

3.2.1. Elements

Elements obtained from Teflon filters were analyzed by an inductively coupled plasma mass spectrometer (ICP-MS, Agilent Technologies, Inc., Model 7500a, Santa Clara, CA, USA). Calibration with reference material (Environmental Calibration Standard, Part 5183-4688, Agilent Technologies, Santa Clara, CA, USA) demonstrated good linearity and sensitivity for the instrument. The relative standard deviation for each measurement (repeated twice) was within 3%. The method detection limits (MDLs) were determined by adding three standard deviations of the blank readings to the average blank values [26]. The elemental species are classified into three categories: crustal elements such as Al, Ca, Fe, and Mg, heavy metal elements including As, Ba, Cr, Cu, Mn, Ni, Pb, Ti, and Zn, and trace elements including the rest of the elemental species such as Cd, Co, P, Sn, Sr, and V. The most important part of the elements was the crustal elements, which accounted for 85.3%, 79.9%, and 78.8 of all the elements at PM_{10} , $PM_{2.1}$, and $PM_{1.1}$, respectively. The crustal elements, heavy metal elements, and trace elements constituted relative fractions varied at different particulate sizes, with higher mass percentages of PM_{10} and coarse particles than that of fine particulate matter. The mass concentrations of most elements showed a decreasing trend with increasing sampling height, especially in coarse particles, implying that elements were mainly emitted from locally ground fugitive and construction dust. The percentages of chemical compositions in PM_{10} , $PM_{10-2.1}$, $PM_{2.1}$, and $PM_{1.1}$ at different sampling heights are shown in Figure 5. According to CD values of elements in Table 2, the CD values for crustal elements such as Al, Ca, Fe, and Mg were generally less than 0.3 in PM_{10} , $PM_{2.1}$, and $PM_{1.1}$ but more than 0.3 in $PM_{10-2.1}$, indicating larger differences of crustal elements between two heights in coarse particles.

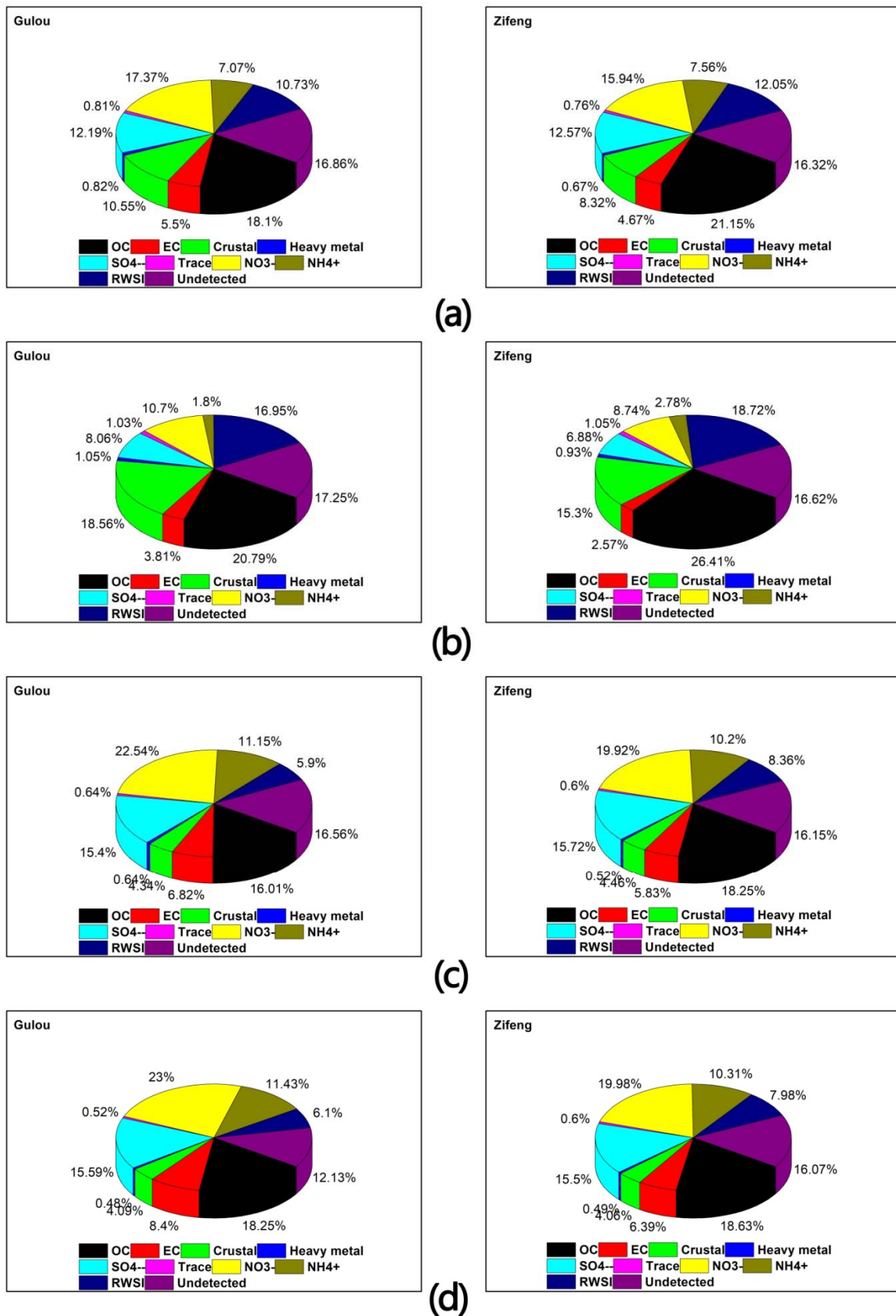


Figure 5. The percentages of chemical compositions in (a) PM₁₀, (b) PM_{10-2.1}, (c) PM_{2.1}, and (d) PM_{1.1} at Gulou and Zifeng.

3.2.2. Water-Soluble Ions

Water-soluble ions are indispensable components in PM, taking a percentage of about 40–50%, especially in fine particles, where there was the largest part of all the compositions. The sulfate, nitrate, ammonium, and the rest of the water-soluble ions (RWSI) accounted for varied from 8.1–15.6%, 10.7–23.0%, 1.8–11.4%, and 5.9–17.0%, respectively, in different particulate sizes at Gulou, and varied from 6.9–15.7%, 8.7–20.0%, 2.8–10.3%, and 8.0–18.7%, respectively, in different particulate sizes at Zifeng. Most of the water-soluble ions showed the characteristics of larger mass concentrations in finer particles, except Na^+ , Ca^{2+} , Mg^{2+} , and F^- , which showed the characteristics of higher mass concentrations in coarse particulate matter. As we know, sea salt was the major source of Na^+ and F^- in coarse particles [49,50]. Therefore, the abundant Na^+ and F^- in coarse particles were mainly from marine salt. However, the sum mass concentrations of Na^+ and F^- in coarse particles only accounted for about 2.56% of the $\text{PM}_{10-2.1}$ mass at the ground level, indicating less contribution from sea salt aerosols to the particulate matter. In total, 88.8% of Ca^{2+} and 76.2% of Mg^{2+} were concentrated in $\text{PM}_{10-2.1}$ at the ground, and the concentrations of Ca^{2+} and Mg^{2+} at Gulou (20 m) were about 100.5% and 52.4% larger than those at Zifeng (380 m), indicating that Ca^{2+} and Mg^{2+} were mainly from the sources of soil and construction dust [51,52] in coarse particles and local ground areas.

To evaluate the equivalence between cations and anions, the cations and anions were calculated based on the following equations, and the ratio of cations/anions (C/A) was applied to estimate the neutralizing level for size-fractionated PM at two heights. The average ratios of cations to anions at Gulou in nine particulate sizes (<0.43 μm , 0.43–0.65 μm , 0.65–1.1 μm , 1.1–2.1 μm , 2.1–3.3 μm , 3.3–4.7 μm , 4.7–5.8 μm , 5.8–9.0 μm , and 9.0–10 μm) were 0.99, 0.94, 0.93, 0.91, 0.98, 1.09, 1.35, 1.66, and 1.92, respectively. In addition, the ratios of C/A at Zifeng in nine particulate sizes from fine to coarse were 1.00, 0.87, 0.91, 0.92, 1.02, 1.05, 0.91, 1.84, and 1.47. Similar neutralizing relationships were shown at different height sites, which implied an acidic tendency of fine particles and an alkaline tendency of coarse particles. The loss of CO_3^{2-} and HCO_3^- , which were not analyzed, is a reason for the deficit of anions in the coarse particles.

$$\text{Cation} = \text{Na}^+ / 23 + \text{K}^+ / 39 + 2 \times \text{Mg}^{2+} / 24 + 2 \times \text{Ca}^{2+} / 40 + \text{NH}_4^+ / 18 + (\text{CH}_3)_2\text{NH}_2^+ / 46 \quad (3)$$

$$\text{Anion} = \text{Cl}^- / 35.5 + \text{F}^- / 19 + \text{NO}_3^- / 62 + 2 \times \text{SO}_4^{2-} / 96 + \text{HCOO}^- / 45 + \text{CH}_3\text{COO}^- / 59 + 2 \times \text{C}_2\text{O}_4^{2-} / 88 \quad (4)$$

In further analysis, the relative contribution of stationary sources such as industrial and powered coal fire to the mobile source for size-fractionated PM was indicated by the ratio of $\text{NO}_3^- / \text{SO}_4^{2-}$ [53,54]. As listed in Table 4, the average mass ratios of $\text{NO}_3^- / \text{SO}_4^{2-}$ were compared at different height levels in different particulate sizes: 1.42, 1.33, 1.46, and 1.48 at Gulou (20 m) and 1.27, 1.27, 1.28, and 1.29 at Zifeng (380 m) in PM_{10} , $\text{PM}_{10-2.1}$, $\text{PM}_{2.1}$, and $\text{PM}_{1.1}$, respectively. The calculated ratios of $\text{NO}_3^- / \text{SO}_4^{2-}$ at Gulou were higher than those at Zifeng, indicating that the mobile source played a relatively more important role to PM at the ground level than at 380 m. The average ratios of $\text{NO}_3^- / \text{SO}_4^{2-}$ at Gulou showed a feature with a larger value of finer particles, suggesting that more contributions from the mobile source were to fine particles than coarse particles, whereas the mean ratios of $\text{NO}_3^- / \text{SO}_4^{2-}$ at Zifeng were similar in PM_{10} , $\text{PM}_{10-2.1}$, $\text{PM}_{2.1}$, and $\text{PM}_{1.1}$, implying that the sources of nitrate and sulfate at higher heights were relatively fixed at different particulate sizes and would be dominantly driven by the secondary formation mechanisms. In addition, higher ratio values of $\text{NO}_3^- / \text{SO}_4^{2-}$ were also found during the pollutant days: 1.44, 1.34, 1.48, and 1.51 at Gulou (20 m) and 1.43, 1.15, 1.48, and 1.54 at Zifeng (380 m) in PM_{10} , $\text{PM}_{10-2.1}$, $\text{PM}_{2.1}$, and $\text{PM}_{1.1}$, respectively, which indicated that the formation of nitrate played an important role under pollutant conditions. Comparing with other studies, the $\text{NO}_3^- / \text{SO}_4^{2-}$ ratios were similar to the work (1.50–0.54) in Beijing at 260 m height before and during the APEC [24] and were higher than those works (0.65–0.86) in Tianjin from

10–220 m height [10,41,54,55], but they were lower than works in Southern California (5.0) and in Denver (2.09) due to the lower usage of sulfur-containing coal in the USA than in China [56–58].

3.2.3. Carbonaceous Components

Carbonaceous species are a very important part of particles. The mass concentrations of size-fractionated OC, EC, and the ratios of OC/EC are shown in Tables 3 and 4 and Figure 6. At ground level, the size distribution of OC was a trimodal mode with peaks at 0.43–0.65 μm , 1.1–2.1 μm , and 4.7–5.8 μm . EC had a bimodal distribution that peaked at <0.43 μm and 5.8–9.0 μm . At the 380 m level, the size distribution of OC was found to be a bimodal mode peaking at 0.43–0.65 μm and 3.3–4.7 μm , while EC only showed a single peak at 0.43–0.65 μm . It could be found that more carbonaceous components were concentrated in fine particulate matter at higher heights. To PM_{10} and $\text{PM}_{10-2.1}$, the mass concentrations of OC and EC were larger at Gulou than Zifeng, indicating a decreasing trend with increased height. Interestingly, in contrast to $\text{PM}_{2.1}$ and $\text{PM}_{1.1}$, the mass concentrations of OC and EC were larger at Zifeng than Gulou, especially the organic acids such as CH_3COO^- and $\text{C}_2\text{O}_4^{2-}$, which could reflect much more influences of the formation mechanism of secondary organic aerosols at the higher level than at the ground. The size-fractionated ratios of OC/EC showed similar trends at Gulou and Zifeng with unimodal distribution. The peak of the OC/EC ratio at Gulou was 3.3–4.7 μm , while at Zifeng the OC/EC ratio peaked at 4.7–5.8 μm . At both sites, the ratios were larger than two, indicating the formation of secondary organic particles [59,60].

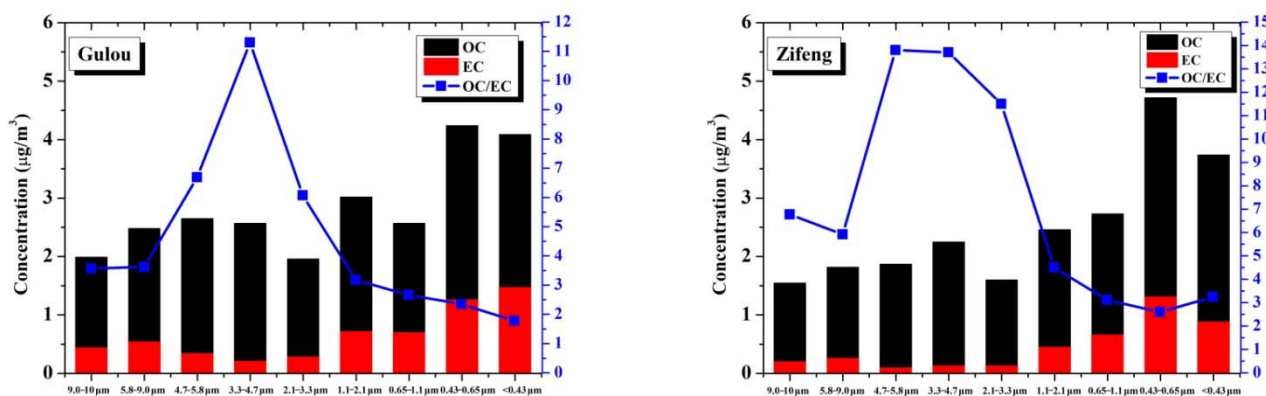


Figure 6. Carbonaceous species and ratios of OC/EC of size-fractionated PM at Gulou (20 m) and Zifeng (380 m).

In addition, the correlation between OC and EC was calculated, which could be a factor of common sources if the value was high. The correlation values (R^2) showed an increasing trend with the particulate size decreased at both sites: 0.80 (PM_{10}) < 0.81 ($\text{PM}_{2.1}$) < 0.91 ($\text{PM}_{1.1}$) at Gulou and 0.68 (PM_{10}) < 0.76 ($\text{PM}_{2.1}$) < 0.79 ($\text{PM}_{1.1}$) at Zifeng. This result suggested that there were common sources of OC and EC in fine particles, while the sources were inconsistent in coarse particles. The OC of coarse PM might be contributed from the hygroscopic growth of water-soluble OC during the transport or the emissions of industrial sources in the regional areas [61]. The EC in the coarse particles could be formed by the resuspension of soil dust and the friction loss of tires [61–63].

Table 3. The average mass concentrations of main chemical compositions at each sampling height in PM₁₀, PM_{10-2.1}, PM_{2.1}, and PM_{1.1} (μg m⁻³).

	Gulou (20 m)				Zifeng (380 m)			
	PM ₁₀	PM _{10-2.1}	PM _{2.1}	PM _{1.1}	PM ₁₀	PM _{10-2.1}	PM _{2.1}	PM _{1.1}
Al	1.24	0.92	0.32	0.20	0.81	0.51	0.30	0.21
Ca	6.80	5.26	1.54	1.10	4.52	3.00	1.52	1.03
Cu	0.07	0.04	0.03	0.018	0.05	0.03	0.02	0.016
Fe	2.64	2.03	0.61	0.38	1.52	0.98	0.54	0.35
Mg	0.74	0.56	0.18	0.10	0.48	0.31	0.17	0.11
Pb	0.07	0.03	0.04	0.020	0.05	0.02	0.03	0.025
V	0.008	0.005	0.004	0.002	0.005	0.002	0.003	0.002
Zn	0.30	0.13	0.17	0.07	0.18	0.08	0.10	0.07
Na ⁺	1.25	0.88	0.37	0.27	1.12	0.64	0.49	0.34
K ⁺	0.94	0.31	0.63	0.46	0.99	0.30	0.69	0.34
Cl ⁻	2.30	1.13	1.17	0.78	1.66	0.80	0.86	0.64
NO ₃ ⁻	18.82	5.06	13.76	9.41	14.03	2.73	11.30	8.94
SO ₄ ²⁻	13.21	3.81	9.40	6.37	11.07	2.16	8.91	6.94
NH ₄ ⁺	7.66	0.85	6.81	4.67	6.66	0.87	5.78	4.61
OC	19.60	9.84	9.77	7.46	18.62	8.28	10.35	8.34
EC	5.96	1.80	4.16	3.44	4.11	0.81	3.30	2.86
CH ₃ COO ⁻	0.61	0.34	0.27	0.18	2.41	1.12	1.29	1.02
HCOO ⁻	0.61	0.43	0.18	0.13	0.42	0.23	0.19	0.15
C ₂ O ₄ ²⁻	0.25	0.15	0.10	0.07	0.43	0.18	0.25	0.20
(CH ₃) ₂ NH ₂ ⁺	0.12	0.06	0.06	0.04	0.09	0.05	0.04	0.03

Table 4. The average ratios of cations/anions, NO₃⁻/SO₄²⁻, and OC/EC for size-fractionated PM.

PM Size	Cations/Anions		NO ₃ /SO ₄ ²⁻		OC/EC	
	GL ^a	ZF ^a	GL	ZF	GL	ZF
<0.43 μm	0.99	1.00	1.44	0.92	1.78	3.24
0.43–0.65 μm	0.94	0.87	1.35	1.42	2.35	2.60
0.65–1.1 μm	0.93	0.91	1.68	1.34	2.66	3.12
1.1–2.1 μm	0.91	0.92	1.44	1.19	3.18	4.50
2.1–3.3 μm	0.98	1.02	1.32	1.39	6.07	11.53
3.3–4.7 μm	1.09	1.05	1.55	1.54	11.30	13.77
4.7–5.8 μm	1.35	0.91	1.15	0.86	6.69	13.87
5.8–9.0 μm	1.66	1.84	1.52	1.34	3.62	5.92
9.0–10 μm	1.92	1.47	1.06	1.04	3.57	6.77
PM ₁₀	1.08	1.01	1.42	1.27	3.29	4.53
PM _{10-2.1}	1.36	1.27	1.33	1.27	5.46	10.28
PM _{2.1}	0.94	0.91	1.46	1.28	2.35	3.13
PM _{1.1}	0.95	0.91	1.48	1.29	2.17	2.92

^a GL represents Gulou site (20 m), ZF represents Zifeng site (380 m).

3.3. Source Apportionment

The source contributions of size-fractionated PM were calculated with the CMB model, which has been widely used in previous studies [64–66]. The source profiles including soil dust, the coal-fired power plant, vehicle exhaust, steel smelting, construction dust, secondary sulfate, secondary nitrate, and fugitive dust were used as model input for the CMB model. These profiles were obtained by previous work in the Yangtze River Delta [18]. Twenty-two species (Al, As, Ba, Ca, Cd, Cr, Cu, Fe, Mg, Mn, Pb, Zn, Ti, V, Cl⁻, NO₃⁻, SO₄²⁻, NH₄⁺, K⁺, Na⁺, OC, and EC), as well as the mass concentrations of size-fractionated PM, were used as ambient data for the CMB calculations. The source contribution estimates (SCEs) of different particulate sizes at Gulou and Zifeng are summarized in Table 5 and are also shown in Figure 7.

Table 5. Source contribution estimates (SCEs) of PM₁₀, PM_{10-2.1}, PM_{2.1}, and PM_{1.1} mass concentrations with CMB model ($\mu\text{g m}^{-3}$).

	Gulou (20 m)				Zifeng (380 m)			
	PM ₁₀	PM _{10-2.1}	PM _{2.1}	PM _{1.1}	PM ₁₀	PM _{10-2.1}	PM _{2.1}	PM _{1.1}
Construction	5.09	2.69	2.41	1.28	3.05	1.22	1.84	1.11
Coal-fired PP	13.84	7.39	6.45	4.09	11.65	4.24	7.41	5.81
Fugitive dust	11.11	6.81	4.30	2.39	6.22	3.66	2.56	1.60
Soil dust	2.77	1.93	0.84	0.55	1.83	0.95	0.88	0.71
Steel smelting	0.79	0.37	0.41	0.22	0.70	0.28	0.42	0.32
Vehicle exhaust	14.74	5.81	8.93	6.10	10.17	3.06	7.12	5.50
Nitrate	19.69	5.98	13.70	10.65	17.88	5.27	12.61	10.47
Sulfate	15.65	5.11	10.54	8.11	15.51	4.38	11.12	9.14
SOA	18.14	8.68	9.47	7.31	17.23	7.54	9.69	7.79
Others	6.51	2.54	3.96	2.12	3.82	0.76	3.06	2.32

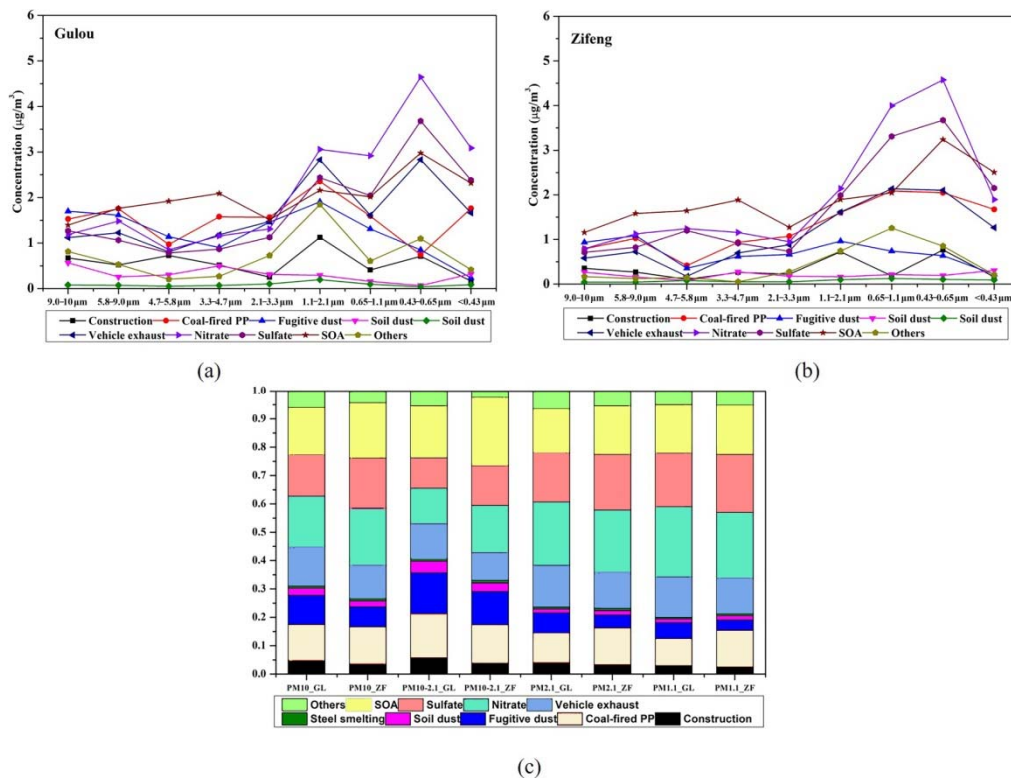


Figure 7. Source contributions of (a) size-fractionated PM at Gulou ($\mu\text{g}/\text{m}^3$), (b) size-fractionated PM at Zifeng ($\mu\text{g}/\text{m}^3$), and (c) PM₁₀, PM_{10-2.1}, PM_{2.1}, and PM_{1.1} at both sites (100%).

The contributions of total emission sources to the size-fractionated PM accounted for varied from 97.3% to 89.9% at Gulou and from 99.2% to 92.2% at Zifeng. The three highest contributors of PM₁₀ were found to keep consistent with nitrate, secondary organic aerosols, and sulfate arranging in order of contribution concentrations. To coarse particles, the three largest sources were secondary organic aerosols, the coal-fired power plant, and fugitive dust at Gulou, whereas the three largest sources were secondary organic aerosols, nitrate, and sulfate at Zifeng, indicating that the ground level would be more influenced by local sources such as fugitive dust, but at higher heights the formations of secondary inorganic and organic aerosols were more important. There was a similar contribution pattern in PM_{2.1} and PM_{1.1} at both heights, and the three largest emissions were nitrate, sulfate, and secondary organic aerosols. Interestingly, the fourth largest emission at Gulou was vehicle exhaust in PM₁₀, PM_{2.1}, and PM_{1.1}, whereas it was the coal-fired power plant

at Zifeng in PM₁₀, PM_{2.1}, and PM_{1.1}, also implying that the local source (vehicle exhaust) influenced more at the ground level.

As shown in Figure 7, the contributions to coarse and fine particulate matter were significantly different for specific sources. The construction dust (3.9–5.7% vs. 3.2–3.9%), fugitive dust (11.7–14.4% vs. 4.5–7.1%), and soil dust (3.0–4.1% vs. 1.4–1.6%) in coarse and fine particles showed larger contributions in the coarse size bin of PM, in which was found a similar tendency with the concentrations of crustal elements described in Section 3.2.1. The contributions of nitrate (12.7–16.8% vs. 22.2–22.5%) and sulfate (10.8–14.0% vs. 17.3–19.6%) in PM_{10-2.1} and PM_{2.1} indicated an increasing trend as the particulate size decreased. However, the source contributions of secondary organic aerosols were 18.3–24.1% of PM_{102.1} and 15.5–17.1% of PM_{2.1}.

As shown in Table 5, the contribution estimates of each source for PM₁₀ and PM_{10-2.1} were larger at Gulou (20 m) than Zifeng (380 m), depending more on the higher concentrations of PM₁₀ and PM_{10-2.1} at Gulou than Zifeng. By contrast, the source contribution estimates for fine particles such as PM_{2.1} and PM_{1.1} showed different features. Dusts, such as construction dust, fugitive dust, and soil dust, contributed a larger amount and proportion at Gulou than Zifeng since these dust sources were from ground and local areas. Vehicle exhaust also contributed larger concentrations at Gulou than Zifeng, which could reflect the influence of heavy traffic at the ground near the sampling site. However, the contributions of sulfate and secondary organic aerosols become larger with higher height, illustrating that the formation mechanisms of secondary aerosols played an important role at the height above the urban canopy. Similarly, the coal-fired power plant and steel smelting also contributed larger concentrations at Zifeng than Gulou, which might be caused not only by the industrial areas in the north of Nanjing but also by the transportation from regional areas. Furthermore, 36 h back trajectories were calculated every three hours for the sampling periods at 20 m and 380 m in this study. A total of 440 trajectories were used for clustering analysis in order to identify common atmospheric transport patterns. All trajectories were categorized into seven and six clusters at 20 m and 380 m, respectively. The average trajectories were shown in Figure 8. It could be found that there were more local sources (clusters two, three, and five in Figure 8a) at 20 m with lower wind speed, while there was more long-distance transportation (clusters one, four, five, and six in Figure 8b) from north of Nanjing with greater wind speed at 380 m.

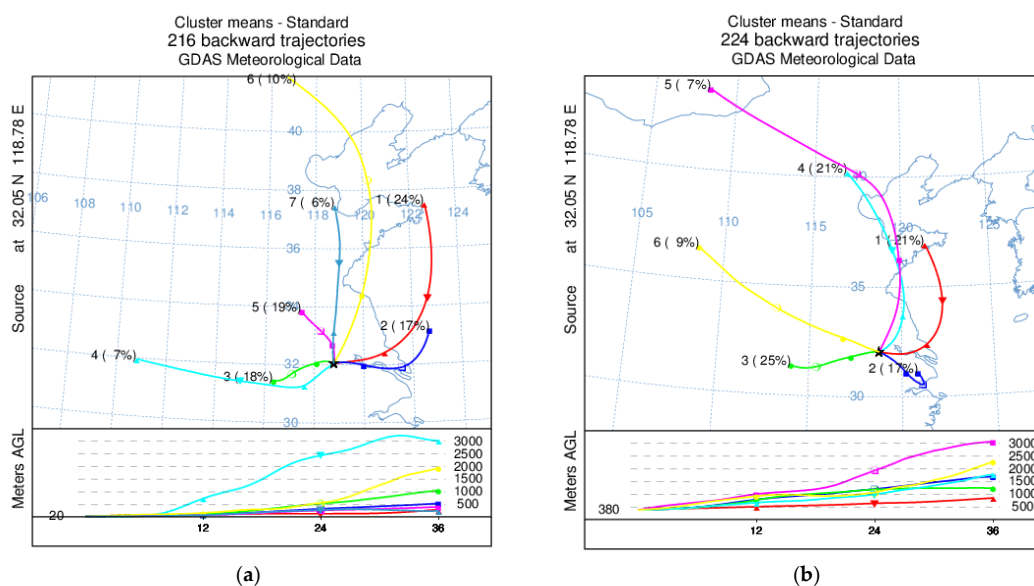


Figure 8. Clustering analysis every three hours for the sampling periods at (a) 20 m and (b) 380 m.

4. Conclusions

The concentrations and chemical compositions of size-fractionated PM were sampled and measured from 16 November to 12 December in 2016 at Gulou (20 m) and Zifeng (380 m) in Nanjing, China. The characteristics of size-fractionated PM mass concentrations at different heights were described and the chemical components including elements, water-soluble ions, and carbonaceous species were analyzed and compared for different particulate sizes and sites. Furthermore, the source apportionment was carried out with the CMB model, and the characteristics of contribution estimates were discussed in this study.

The concentrations of PM₁₀ and PM_{2.1} were $108.3 \pm 23.4 \mu\text{g m}^{-3}$ and $61.0 \pm 18.8 \mu\text{g m}^{-3}$ at Gulou and were $88.1 \pm 21.1 \mu\text{g m}^{-3}$ and $56.7 \pm 18.6 \mu\text{g m}^{-3}$ at Zifeng, which indicated a decreasing trend as the height increased. In contrast, the concentrations of PM_{1.1} were $40.9 \pm 13.0 \mu\text{g m}^{-3}$ and $44.8 \pm 15.8 \mu\text{g m}^{-3}$ at Gulou and Zifeng, indicating particles congregating in a finer particulate size bin at the higher level. The PM pollutant days were relative to the weather conditions, especially when wind speed was low.

All the species of size-fractionated PM detected in this study accounted for 82.7–87.9% of the total PM mass concentrations at Gulou and accounted for 83.1–83.4% at Zifeng. The crustal elements were concentrated more in coarse particles, accounting for 18.6% and 15.3% at Gulou and Zifeng. The water-soluble ions, especially nitrate (8.7–23.0%), sulfate (6.9–15.6%), and ammonium (1.8–11.4%), were dominant components of size-fractionated PM. The concentrations of nitrate, sulfate, and ammonium showed an increasing tendency with decreasing particulate size. Organic carbon was another dominant component of size-fractionated PM, accounting for 16.0–20.8% and 18.3–26.4%, respectively, at Gulou and Zifeng, which indicated larger contributions at the higher level.

The source contribution estimates (SCEs) calculated by the CMB model showed that the secondary inorganic and organic aerosols were the largest three contributors of PM₁₀, PM_{2.1}, and PM_{1.1} at both sites, but the fourth largest sources at Gulou and Zifeng were vehicle exhaust and the coal-fired power plant, respectively. To PM_{10-2.1}, the largest three contributors at Gulou were secondary organic aerosols, the coal-fired power plant, and fugitive dust, which was different with Zifeng. Zifeng showed secondary organic aerosols, nitrate, and sulfate as the largest sources of PM_{10-2.1}. These results illustrated that dusts including construction dust, fugitive dust, soil dust, and vehicle exhaust would contribute more at the ground level. In recent years, concentrations were decreased by 41.4%, 26.3%, and 24.8% of PM₁₀, PM_{2.1}, and PM_{1.1} in this study compared to the winter of 2010 at the same sampling site. These results showed an encouraging improvement in the control of particulate matter in Nanjing.

Author Contributions: Conceptualization, T.W. and H.W.; data curation, P.C.; funding acquisition, T.W.; investigation, M.X. and B.Z.; methodology, S.L. and M.L.; supervision, H.W.; visualization, P.C. and H.W.; writing—original draft, H.W. All authors have read and agreed to the published version of the manuscript.

Funding: This work was supported by the National Natural Science Foundation of China (42077192, 41621005), the National Key Basic Research and Development Program of China (2020YFA0607802, 2019YFC0214603) and the Emory University-Nanjing University Collaborative Research Grant.

Institutional Review Board Statement: Not applicable.

Conflicts of Interest: The authors declare no conflict of interest.

References

1. Rohr, A.C.; Wyzga, R.E. Attributing health effects to individual particulate matter constituents. *Atmos. Environ.* **2012**, *62*, 130–152. [[CrossRef](#)]
2. Ma, J.; Chen, L.L.; Guo, Y.; Wu, Q.; Yang, M.; Wu, M.H. Phthalate diesters in Airborne PM_{2.5} and PM₁₀ in a suburban area of Shanghai: Seasonal distribution and risk assessment. *Sci. Total Environ.* **2014**, *497*, 467–474. [[CrossRef](#)] [[PubMed](#)]
3. Intergovernmental Panel on Climate Change (IPCC). 2006. Available online: <http://www.ipcc-nggip.iges.or.jp/public/2006gl/index.html> (accessed on 26 May 2022).

4. Isaksen, I.S.; Granier, C.; Myhre, G.; Berntsen, T.K.; Dalsøren, S.B.; Gauss, M.; Klimonth, Z.; Benestad, R.; Bousquet, P.; Collins, W.; et al. Atmospheric composition change: Climate—Chemistry interactions. *Atmos. Environ.* **2009**, *43*, 5138–5192. [[CrossRef](#)]
5. Ramachandran, S.; Kedia, S. Black carbon aerosols over an urban region: Radiative forcing and climate impact. *J. Geophys. Res. Atmos.* **2010**, *115*, D10202. [[CrossRef](#)]
6. Watson, J.G. Visibility: Science and regulation. *J. Air Waste Manag. Assoc.* **2002**, *52*, 628–713. [[CrossRef](#)] [[PubMed](#)]
7. Ying, Q.; Mysliwiec, M.; Kleeman, M.J. Source apportionment of visibility impairment using a three-dimensional source-oriented air quality model. *Environ. Sci. Technol.* **2014**, *38*, 1089–1101. [[CrossRef](#)]
8. Sun, Y.L.; Zhuang, G.; Tang, A.; Wang, Y.; An, Z. Chemical characteristics of PM_{2.5} and PM₁₀ in haze-fog episodes in Beijing. *Environ. Sci. Technol.* **2006**, *40*, 3148–3155. [[CrossRef](#)]
9. Zhao, X.J.; Zhao, P.S.; Xu, J.; Meng, W.; Pu, W.; Dong, F.; He, D.; Shi, Q. Analysis of a winter regional haze event and its formation mechanism in the North China Plain. *Atmos. Chem. Phys.* **2013**, *13*, 5685–5696. [[CrossRef](#)]
10. Wu, H.; Zhang, Y.; Han, S.; Wu, J.; Bi, X.; Shi, G.; Wang, J.; Yao, Q.; Cai, Z.; Liu, J.; et al. Vertical characteristics of PM_{2.5} during the heating season in Tianjin, China. *Sci. Total Environ.* **2015**, *523*, 152–160. [[CrossRef](#)]
11. Tie, X.; Cao, J. Aerosol pollution in China: Present and future impact on environment. *Particuology* **2009**, *7*, 426–431. [[CrossRef](#)]
12. Zheng, M.; Wang, F.; Hagler, G.; Hou, X.; Bergin, M.; Cheng, Y. Sources of excess urban carbonaceous aerosol in the Pearl River Delta Region, China. *Atmos. Environ.* **2011**, *45*, 1175–1182. [[CrossRef](#)]
13. Wang, L.T.; Wei, Z.; Yang, J.; Zhang, Y.; Zhang, F.; Su, J.; Meng, C.; Zhang, Q. The 2013 severe haze over the southern Hebei, China: Model evaluation, source apportionment, and policy implications. *Atmos. Chem. Phys.* **2014**, *14*, 3151–3173. [[CrossRef](#)]
14. Choi, K.; Chong, K. Modified Inverse Distance Weighting Interpolation for Particulate Matter Estimation and Mapping. *Atmosphere* **2022**, *13*, 846. [[CrossRef](#)]
15. Wu, H.; Wang, T.; Wang, Q.; Cao, Y.; Qu, Y.; Nie, D. Radiative effects and chemical compositions of fine particles modulating urban heat island in Nanjing, China. *Atmos. Environ.* **2021**, *247*, 118201. [[CrossRef](#)]
16. Zhang, Y.; Xu, H.; Tian, Y.; Shi, G.L.; Zeng, F.; Wu, J. The study on vertical variability of PM₁₀ and the possible sources on a 220 m tower, in Tianjin, China. *Atmos. Environ.* **2011**, *45*, 6133–6140. [[CrossRef](#)]
17. Quan, J.; Tie, X.; Zhang, Q.; Liu, Q.; Li, X.; Gao, Y. Characteristics of heavy aerosol pollution during the 2012–2013 winter in Beijing, China. *Atmos. Environ.* **2014**, *88*, 83–89. [[CrossRef](#)]
18. Chen, P.; Wang, T.; Dong, M.; Kasoar, M.; Han, Y.; Xie, M.; Li, S.; Zhuang, B.; Li, M.; Huang, T. Characterization of major natural and anthropogenic source profiles for size-fractionated PM in Yangtze River Delta. *Sci. Total Environ.* **2017**, *598*, 135–145. [[CrossRef](#)]
19. Kanakidou, M.; Seinfeld, J.H.; Pandis, S.N.; Barnes, I.; Dentener, F.J.; Facchini, M.C.; Van Dingenen, R.; Ervens, B.; Nenes, A.; Nielsen, C.J.; et al. Organic aerosol and global climate change modeling: A review. *Atmos. Chem. Phys.* **2005**, *5*, 1053–1123. [[CrossRef](#)]
20. Zhang, Q.; Jimenez, J.L.; Canagaratna, M.R.; Allan, J.D.; Coe, H.; Ulbrich, I.; Alfarra, M.R.; Takami, A.; Middlebrook, A.M.; Sun, Y.L.; et al. Ubiquity and dominance of oxygenated species in organic aerosols in anthropogenically influenced Northern Hemisphere midlatitudes. *Geophys. Res. Lett.* **2007**, *34*, L13801. [[CrossRef](#)]
21. Shi, G.; Tian, Y.; Han, S.; Zhang, Y.; Li, X.; Feng, Y.; Wu, J.; Zhu, T. Vertical characteristics of carbonaceous species and their source contributions in a Chinese mega city. *Atmos. Environ.* **2012**, *60*, 358–365. [[CrossRef](#)]
22. Han, S.; Zhang, Y.; Wu, J.; Zhang, X.; Tian, Y.; Wang, Y.; Ding, J.; Yan, W.; Bi, X.; Shi, G.; et al. Evaluation of regional background particulate matter concentration based on vertical distribution characteristics. *Atmos. Chem. Phys.* **2015**, *15*, 11165–11177. [[CrossRef](#)]
23. Sun, Y.; Chen, C.; Zhang, Y.; Xu, W.; Zhou, L.; Cheng, X.; Zheng, H.; Ji, D.; Li, J.; Tang, X.; et al. Rapid formation and evolution of an extreme haze episode in Northern China during winter 2015. *Sci. Rep.* **2016**, *6*, 27151. [[CrossRef](#)]
24. Chen, P.; Wang, T.; Hu, X.; Xie, M. Chemical mass balance source apportionment of size-fractionated particulate matter in Nanjing, China. *Aerosol Air Qual. Res.* **2015**, *15*, 1855–1867. [[CrossRef](#)]
25. Chen, P.; Wang, T.; Lu, X.; Yu, Y.; Kasoar, M.; Xie, M.; Zhuang, B. Source apportionment of size-fractionated particles during the 2013 Asian Youth Games and the 2014 Youth Olympic Games in Nanjing, China. *Sci. Total Environ.* **2017**, *579*, 860–870. [[CrossRef](#)]
26. Zhang, W.; Zhang, Y.; Lv, Y.; Li, K.; Li, Z. Observation of atmospheric boundary layer height by round-based LiDAR during haze days. *J. Remote Sens.* **2013**, *17*, 981–992.
27. Chow, J.; Watson, J. Review of PM_{2.5} and PM₁₀ apportionment for fossil fuel combustion and other sources by the chemical mass balance receptor model. *Energy Fuels* **2002**, *16*, 222–260. [[CrossRef](#)]
28. Deng, J.; Zhang, Y.; Qiu, Y.; Zhang, H.; Du, W.; Xu, L.; Hong, Y.; Chen, Y.; Chen, J. Source apportionment of PM_{2.5} at the Lin'an regional background site in China with three receptor models. *Atmos. Res.* **2018**, *202*, 23–32. [[CrossRef](#)]
29. Wang, H.; Zhuang, Y.; Wang, Y.; Sun, Y.; Yuan, H.; Zhuang, G. Long-term monitoring and source apportionment of PM_{2.5}/PM₁₀ in Beijing, China. *J. Environ. Sci.* **2008**, *20*, 1323–1327. [[CrossRef](#)]
30. Xie, S.; Liu, Z.; Chen, T.; Hua, L. Spatiotemporal variations of ambient PM₁₀ source contributions in Beijing in 2004 using positive matrix factorization. *Atmos. Chem. Phys.* **2008**, *8*, 2701–2716. [[CrossRef](#)]
31. Yao, L.; Yang, L.; Yuan, Q.; Yan, C.; Dong, C.; Meng, C. Source apportionment of PM_{2.5} in a background site in the North China Plain. *Sci. Total Environ.* **2016**, *541*, 590–598. [[CrossRef](#)]

32. Stohl, A. Trajectory statistics—A new method to establish source-receptor relationships of air pollutants and its application to the transport of particulate sulfate in Europe. *Atmos. Environ.* **1996**, *30*, 579–587. [[CrossRef](#)]
33. Hwang, I.; Hopke, P. Estimation of source apportionment and potential source locations of PM_{2.5} at a west coastal IMPROVE site. *Atmos. Environ.* **2007**, *41*, 506–518. [[CrossRef](#)]
34. Yang, Y.; Zheng, X.; Gao, Z.; Wang, H.; Wang, T.; Li, Y.; Lau, G.; Yim, S. Long-Term Trends of Persistent Synoptic Circulation Events in Planetary Boundary Layer and Their Relationships with Haze Pollution in Winter Half Year over Eastern China. *J. Geophys. Res. Atmos.* **2018**, *123*, 10991–11007. [[CrossRef](#)]
35. Yang, Y.; Yim, S.H.; Haywood, J.; Osborne, M.; Chan, J.C.; Zeng, Z.; Cheng, J.C. Characteristics of Heavy Particulate Matter Pollution Events over Hong Kong and Their Relationships with Vertical Wind Profiles Using High-Time-Resolution Doppler Lidar Measurements. *J. Geophys. Res. Atmos.* **2019**, *124*, 9609–9623. [[CrossRef](#)]
36. Xue, M.; Ma, J.; Yan, P.; Pan, X. Impacts of pollution and dust aerosols on the atmospheric optical properties over a polluted rural area near Beijing city. *Atmos. Res.* **2011**, *101*, 835–843. [[CrossRef](#)]
37. Chow, J.; Watson, J.; Pritchett, L.; Pierson, W.; Frazier, C.; Purcell, R. The dri thermal/optical reflectance carbon analysis system: Description, evaluation and applications in U.S. air quality studies. *Atmos. Environ.* **1993**, *27*, 1185–1201. [[CrossRef](#)]
38. Chow, J.; Watson, J.; Chen, L.; Arnott, W.; Moosmuller, H. Equivalence of elemental carbon by thermal/optical reflectance and transmittance with different temperature protocols. *Environ. Sci. Technol.* **2004**, *38*, 4414–4422. [[CrossRef](#)]
39. Draxler, R.; Rolph, G. *HYSPLIT (Hybrid Single-Particle Lagrangian Integrated Trajectory) Model*; Access via NOAA ARL READY Website; NOAA Air Resources Laboratory: Silver Spring, MD, USA, 2012, Available online: <http://ready.arl.noaa.gov/HYSPLIT.php> (accessed on 26 May 2022).
40. Draxler, R.; Stunder, B.; Rolph, G.; Stein, A.; Taylor, A. *HYSPLIT4 User's Guide*, version 4; Report; NOAA: Silver Spring, MD, USA, 2012.
41. Wang, J.; Zhou, M.; Liu, B.; Wu, J.; Peng, X.; Zhang, Y.; Han, S.; Feng, Y.; Zhu, T. Characterization and source apportionment of size-segregated atmospheric particulate matter collected at ground level and from the urban canopy in Tianjin. *Environ. Pollut.* **2016**, *219*, 982–992. [[CrossRef](#)]
42. Wongphatarakul, V.; Friedlander, S.; Pinto, J. A comparative study of PM_{2.5} ambient aerosol chemical databases. *Environ. Sci. Technol.* **1998**, *32*, 3926–3934. [[CrossRef](#)]
43. Wilson, J.; Kingham, S.; Sturman, A. Intraurban variations of PM₁₀ air pollution in Christchurch, New Zealand, Implications for epidemiological studies. *Sci. Total Environ.* **2006**, *367*, 2–3. [[CrossRef](#)]
44. Hwang, I.; Hopke, P.; Pinto, J. Source apportionment and spatial distributions of coarse particles during the regional air pollution study. *Environ. Sci. Technol.* **2008**, *42*, 3524–3530. [[CrossRef](#)] [[PubMed](#)]
45. Amato, F.; Alastuey, A.; Rosa, J.; Castanedo, Y.; Campa, A.; Pandolfi, M.; Lozano, A.; Gonzalez, J.; Querol, X. Trends of road dust emission contributions on ambient air particulate levels at rural, urban and industrial sites in southern Spain. *Atmos. Chem. Phys.* **2014**, *14*, 3533–3544. [[CrossRef](#)]
46. Jia, Y.; Rahn, K.; He, K.; Wen, T.; Wang, Y. A novel technique for quantifying the regional component of urban aerosol solely from its sawtooth cycles. *J. Geophys. Res.* **2008**, *113*, D21309. [[CrossRef](#)]
47. Guo, S.; Hu, M.; Zamora, M.; Peng, J.; Shang, D.; Zheng, J.; Du, Z.; Wu, Z.; Shao, M.; Zeng, L. Elucidating severe urban haze formation in China. *Proc. Natl. Acad. Sci. USA* **2014**, *111*, 17373–17378. [[CrossRef](#)]
48. Sun, Y.; Jiang, Q.; Wang, Z.; Fu, P.; Li, J.; Yang, T.; Yin, Y. Investigation of the sources and evolution processes of severe haze pollution in Beijing in January 2013. *J. Geophys. Res. Atmos.* **2014**, *119*, 4380–4398. [[CrossRef](#)]
49. Herner, J.; Ying, Q.; Aw, J.; Gao, O.; Chang, D.; Kleeman, M. Dominant mechanisms that shape the airborne particle size and composition in central California. *Aerosol Sci. Technol.* **2006**, *40*, 827–844. [[CrossRef](#)]
50. Kumar, A.; Sarin, M.M.; Sudheer, A.K. Mineral and anthropogenic aerosols in Arabian Sea-atmospheric boundary layer: Sources and spatial variability. *Atmos. Environ.* **2008**, *42*, 5169–5181. [[CrossRef](#)]
51. Arimoto, R.; Duce, R.; Savoie, D.; Prospero, J.; Talbot, R.; Cullen, J.; Tomza, U.; Lewis, N.; Ray, B. Relationships among aerosol compositions from Asia and the North Pacific during Pem-West. *J. Geophys. Res.* **1996**, *101*, 2011–2023. [[CrossRef](#)]
52. Wang, Y.; Zhuang, G.; Tang, A.; Yuan, H.; Sun, Y.; Chen, S.; Zheng, A. The ion chemistry and source of PM_{2.5} aerosol in Beijing. *Atmos. Environ.* **2005**, *39*, 3771–3784. [[CrossRef](#)]
53. Gao, X.; Yang, L.; Cheng, S.; Gao, R.; Zhou, Y.; Xue, L.; Shou, Y.; Wang, J.; Wang, X.; Nie, W.; et al. Semi-continuous measurement of water-soluble ions in PM_{2.5} in Jinan, China: Temporal variations and source apportionments. *Atmos. Environ.* **2011**, *45*, 6048–6056. [[CrossRef](#)]
54. Tian, Y.Z.; Shi, G.L.; Han, S.; Zhang, Y.; Feng, Y.; Liu, G.R.; Gao, L.; Wu, J.; Zhu, T. Vertical characteristics of levels and potential sources of water-soluble ions in PM₁₀ in a Chinese megacity. *Sci. Total Environ.* **2013**, *447*, 1–9. [[CrossRef](#)] [[PubMed](#)]
55. Zhang, T.; Cao, J.; Tie, X.; Shen, Z.; Liu, S.; Ding, H.; Han, Y.M.; Wang, G.H.; Ho, K.F.; Qiang, J.; et al. Water-soluble ions in atmospheric aerosols measured in Xi'an, China: Seasonal variations and sources. *Atmos. Res.* **2011**, *102*, 110–119. [[CrossRef](#)]
56. Kim, B.; Teffera, S.; Zeldin, M. Characterization of PM_{2.5} and PM₁₀ in the South Coast Air Basin of Southern California: Part 1—spatial variations. *J. Air. Waste Manag. Assoc.* **2000**, *50*, 2034–2044. [[CrossRef](#)] [[PubMed](#)]
57. Yao, X.; Chan, C.; Fang, M.; Cadle, S.; Chan, T.; Mulawa, P.; He, K.; Ye, B. The water-soluble ionic composition of PM_{2.5} in Shanghai and Beijing, China. *Atmos. Environ.* **2002**, *36*, 4223–4234. [[CrossRef](#)]

58. Ozturk, F.; Bahreini, R.; Wagner, N.; Dubé, W.P.; Young, C.J.; Brown, S.S.; Brock, C.A.; Ulbrich, I.M.; Jimenez, J.L.; Cooper, O.R.; et al. Vertically resolved chemical characteristics and sources of submicron aerosols measured on a Tall Tower in a suburban area near Denver, Colorado in winter. *J. Geophys. Res.* **2013**, *118*, 13591–13605. [[CrossRef](#)]
59. Turpin, B.; Cary, R.; Huntzicker, J. An in-situ, time-resolved analyzed for aerosol organic and elemental carbon. *Aerosp. Sci. Technol.* **1990**, *12*, 161–171. [[CrossRef](#)]
60. Castro, L.M.; Pio, C.A.; Harrison, R.; Smith, D. Carbonaceous aerosol in urban and rural European atmospheres, estimation of secondary organic carbon concentrations. *Atmos. Environ.* **1999**, *33*, 2771–2781. [[CrossRef](#)]
61. Wang, H.L.; Zhu, B.; An, J.L.; Duan, Q.; Zou, J.N.; Shen, L.J. Size distribution and characterization of OC and EC in atmospheric aerosols during the Asian youth games of Nanjing, China. *J. Environ. Sci.* **2014**, *35*, 3271–3279. (In Chinese)
62. Shah, S.; Cocker, D.; Miller, J.; Norbeck, J. Emission rates of particulate matter and elemental and organic carbon from In-use diesel engines. *Environ. Sci. Technol.* **2004**, *38*, 2544–2550. [[CrossRef](#)]
63. Lan, Z.; Chen, D.; Li, X.; Huang, X.; He, L.; Denga, Y.; Feng, N.; Hu, M. Modal characteristics of carbonaceous aerosol size distribution in an urban atmosphere of South China. *Atmos. Res.* **2011**, *100*, 51–60. [[CrossRef](#)]
64. Chow, J.C.; Watson, J.; Lowenthal, D. Sources and chemistry of PM₁₀ aerosol in Santa Barbara County, CA. *Atmos. Environ.* **1996**, *30*, 1489–1499. [[CrossRef](#)]
65. Feng, Y.; Bai, Z.; Zhu, T. The principle and application of improved-source-apportionment technique of atmospheric particulate matter Chinese. *J. Environ. Sci.* **2002**, *23*, 106–108.
66. Shi, G.; Feng, Y.; Zeng, F.; Li, X.; Zhang, Y.; Wang, Y. Use of a nonnegative constrained principal component regression chemical mass balance model to study the contributions of nearly collinear sources. *Environ. Sci. Technol.* **2009**, *43*, 8867–8873. [[CrossRef](#)] [[PubMed](#)]